The final publication is available at

http://dx.doi.org/10.1016/j.corsci.2012.06.012

THERMOGALVANIC EFFECTS ON THE CORROSION OF COPPER IN HEAVY BRINE LiBr SOLUTIONS

Fernández-Domene, R.M., Blasco-Tamarit, E., García-García, D.M., García-Antón, J. *

Ingeniería Electroquímica y Corrosión (IEC). Departamento de Ingeniería Química y Nuclear. ETSI Industriales. Universidad Politécnica de Valencia. P.O. Box 22012, E-46071 Valencia. Spain.

Tel. 34-96-387 76 30, Fax. 34-96-387 76 39, e-mail. jgarciaa@iqn.upv.es

Thermogalvanic corrosion of copper in heavy brine LiBr solutions has been investigated using a zero-resistance ammeter (ZRA). The temperature gradients between copper electrodes immersed in the same LiBr solution result in the formation of thermogalvanic cells with hot anodes, leading to high and sustained thermogalvanic currents. Copper loss rates, calculated using Faraday's law, substantially exceed $0.025 \text{ mm year}^{-1}$, a value regarded as the threshold of low corrosion rates. The effects of thermogalvanic coupling on the surface properties of the anode and the cathode have been analysed by means of electrochemical impedance spectroscopy (EIS). The results obtained in this analysis have been related to the process of copper electrodissolution in bromide media.

Keywords: A. Copper; B. EIS, polarisation; C. Anodic dissolution

INTRODUCTION

In recent years, interest in absorption refrigeration technology has been growing because these systems use pairs of refrigerants and absorbents which do not deplete the ozone layer. Moreover, waste heat or solar energy can be used for their operation, thus helping to control global warming [1-3]. Lithium bromide (LiBr) solutions are widely used as refrigerants for absorption-type air-conditioning and industrial drying systems due to their good thermodynamic properties [3-6].

Copper has been used as the structural material of heat exchangers because of its excellent thermal conductivity and good corrosion resistance. Refrigeration systems based on absorption phenomena include copper and copper alloys in the system design [5, 7-9]. Since it is impossible to design heat exchangers where all the surfaces are isothermal, temperature differences on the same metal surface in contact with the same electrolyte solution can produce sufficient electrode potential differences to give rise to the formation of a thermogalvanic cell, which leads to thermogalvanic corrosion. Electrode potentials change with temperature, but temperature changes may also affect the kinetics of dissolution, in particular activation-controlled processes. Boden [10] reported that the electrode potential of copper electrodes in a NaCl solution became more anodic as temperature increased, creating a substantial thermogalvanic corrosion cell and enhancing corrosion rates. Bell *et. al.* [11] also obtained hot anodes when investigating thermogalvanic corrosion of copper pipes in a 3% NaCl solution.

Bromide solutions are highly corrosive and attack the copper parts of the absorption system [7-9, 12-16]. Thus, the existence of zones with different temperatures inside the heat exchangers can aggravate the corrosion of copper in the LiBr solutions.

2

Furthermore, the presence of Cu^{2+} in lithium bromide refrigerants resulting from the corrosion of copper equipment can cause the galvanic corrosion of ferrous parts in absorption systems [6].

This work studies the thermogalvanic behaviour of copper in heavy brine LiBr solutions imposing temperature gradients up to 75 degrees.

EXPERIMENTAL PROCEDURE

The working electrodes were copper cylindrical probes (99.9% purity), 8 mm in diameter, with a total surface area of 0.5 cm^2, covered with a 2-mm polytetrafluoroethylene (PTFE) coating. The electrodes were wet abraded using 500-, 1000- and 4000-grade silicon carbide (SiC) emery papers, and rinsed with distilled water. Aqueous solutions of 400 g/l (4.61 M), 700 g/l (8.06 M) and 992 g/l (11.42 M) LiBr were used.

The polarisation tests were determined using an Autolab PGSTAT302N potentiostat, in the three LiBr solutions mentioned above (400, 700 and 992 g/l LiBr), at four different temperatures (25, 50, 75 and 100º C; the maximum temperature in the 400 g/l LiBr solution was 75º C, since at 100º C the solution showed signs of boiling). The potentials of the working electrode were measured against a silver-silver chloride (Ag/AgCl 3M KCl) reference electrode. The auxiliary electrode was a platinum (Pt) wire. Dissolved oxygen was removed from the LiBr solutions by bubbling N_2 and the purging continued during the tests over the electrolyte. Polarisation tests began at a potential value of −50 $mV_{Ag/AgCl}$ with respect to the open circuit potential and the potential was subsequently

scanned anodically to 1 $V_{Ag/AgCl}$ at a scanning rate of 0.5 mV/s. Corrosion current densities (i_{corr}) and corrosion potentials (E_{corr}) were estimated from these curves and information about the general electrochemical behaviour of copper in the LiBr solutions at different temperatures was obtained.

The experimental arrangement used to study thermogalvanic corrosion is shown in **Figure 1**. The temperature difference between each half-cell is obtained by cooling directly one side and heating the other side using two thermostated baths. Electrolytic contact is achieved through a sintered glass membrane (porosity 3, with an internal resistance of 5-10 Ω) fitted between the two compartments. The sintered glass membrane acts as a thermal and diffusional barrier between both half-cells, which prevents the hot and cold electrolytes from mixing and over which the stable temperature gradient occurs [17-22]. Thermogalvanic corrosion tests were performed at four different temperatures in the hot half-cell, namely 25, 50, 75 and 100º C (when using the 400 g/l LiBr solution, the maximum temperature was 75º C, since at 100º C the solution started boiling), while the cold half-cell was always at 25º C. Measurements were carried out in an inert atmosphere by purging N_2 over the electrolyte solution, which was deaerated previously for 20 minutes.

Thermogalvanic corrosion was studied by using the potentiostat as a Zero Resistance Ammeter (ZRA) (**Figure 1**). This procedure consists of connecting the cold and hot copper electrodes (WE1 and WE2, respectively) and recording current variations with time between them with the ZRA. Simultaneously, the potential of this couple is measured against a Ag/AgCl reference electrode. The sign convention of the ZRA was that when the hot electrode (WE2) was anodic with respect to the cold electrode (WE1),

the ZRA current was negative. ZRA current and potential data were recorded for 6 hours.

The EIS measurements were performed before and after the 6 hours of open circuit measurements (ZRA) at the open circuit potential value, in order to study the effects of the thermogalvanic couple on the electrolyte/metal interface. The voltage perturbation amplitude was 10 mV in the frequency range of 100 kHz to 10 mHz. The conditions of the EIS experiments were the same as those in the ZRA tests.

RESULTS AND DISCUSSION

Potentiodynamic tests

Potentiodynamic polarisation curves for copper in the 700 g/l LiBr solution at different temperatures (25, 50, 75 and 100º C) are presented in **Figure 2**. These curves are representative of polarisation curves for copper in heavy brine LiBr solutions, so curves for copper in the 400 and 992 g/l LiBr solutions are not presented here. Different anodic regions can be observed in the curves, as reported in the literature for copper in halide solutions [7, 12, 15, 23-32].

Region 1: apparent Tafel behaviour region.

Above the corrosion potential, E_{corr}, there is a region of active copper dissolution known as apparent Tafel behaviour region, where current density increases linearly with potential with a slope close to 60 mV dec^{-1} [7, 12, 15, 24-27, 31]. The anodic process ocurring in this region is the formation of soluble complexes in the form of CuX_2^- ($CuBr_2^-$ in bromide solutions) and can be attributed to a two-stage process: a charge

transfer reaction at the electrode/electrolyte interface (eqs. 1a and 1b), and the diffusion

of $CuBr_2^-$ from the electrode surface towards the solution bulk (eq. 2), according to [7,

15, 23-26, 29-35]:

$$Cu + Br^- \Leftrightarrow CuBr_{ads} + e^- \tag{1a}$$

$$CuBr_{ads} + Br^- \rightarrow \left(CuBr_2^-\right)_s \tag{1b}$$

$$\left(CuBr_2^-\right)_s \rightarrow \left(CuBr_2^-\right)_e \tag{2}$$

Where subscripts "ads", "s" and "e" indicate adsorbed species, electrode surface and

electrolyte, respectively. The process of copper dissolution is therefore under mixed

control, that is, it is controlled both by the electrodissolution process and the diffusion

of complex $CuBr_2^-$ species from the outer Helmholtz plane (*OHP*) towards the

electrolyte through the diffusion layer [7, 23, 31, 36-39].

It can be observed in **Figure 2** that current density values within this first region

increase with increasing temperature. As it is widely known, charge and mass transfer

rates increase with temperature; therefore, as temperature increases, the reactions

described above are enhanced and current density values increase.

Region 2: maximum and limit current density region.

A current density maximum is observed beyond the apparent Tafel behaviour region.

This current density peak and its subsequent decrease can be associated with the

formation and growth of a porous and very insoluble layer of CuX (CuBr in bromide

solutions) on the copper surface [23-25, 31, 33, 34, 40-42], according to the following equations:

$$Cu + Br^- \Leftrightarrow CuBr + e^- \tag{3}$$

$$Cu + CuBr_2^- \Leftrightarrow 2CuBr + e^- \tag{4}$$

The amount of CuBr increases with time, forming a layer that can make current density and, consequently, corrosion rate decrease, in spite of having no protective properties. The minimum value reached by current density after the peak indicates a maximum coverage of the surface by the CuBr layer [38]. As copper keeps reacting with bromide ions to form more CuBr, the reaction rate decreases and equals the diffusion rate of bromide ions from the bulk solution to the electrode surface. After that, bromide diffusion becomes the rate-controlling step and current density reaches an approximately constant value (limit current density) within a potential range [12, 25, 33, 34, 38, 43]. Because of the high current density values recorded in this second region, the corrosion product layer cannot be regarded as a true passive film [37].

It is noteworthy that as the temperature of the solution increases, the current density peak is less discernible, disappearing at 100º C, where no current density minimum is observed. Moreover, current density values increase in this region with increasing temperatures. Therefore, it can be said that higher temperatures make the layer of CuBr weaker.

Region 3: high potential region.

In the third region of polarisation curves, at potentials beyond the limit current density region, the CuBr layer undergoes further dissolution. Two competitive reactions have been suggested for this dissolution [24, 25, 34]:

$$CuBr + Br^- \rightarrow CuBr_2^-$$ **(5)**

and

$$CuBr \rightarrow Cu^{2+} + Br^- + e^-$$ **(6)**

Since solubility of CuBr is very low, its dissolution occurs mainly due to complexation reaction, eq. (5). At the same time, the complex species $CuBr_2^-$ dissolves to give Cu^{2+} ions [15, 24, 34]:

$$CuBr_2^- \rightarrow Cu^{2+} + 2Br^- + e^-$$ **(7)**

In addition to the dissolution of the CuBr layer due to bromide ions action, at these high potentials the formation of Cu (II) species from CuBr and $CuBr_2^-$ takes place [15, 24-26, 38, 44]. Among the predominant Cu (II) compounds at high potential values, copper oxide, CuO, is rather common [15, 40, 43].

From the potentiodynamic polarisation curves, corrosion potentials (E_{corr}), corrosion current densities (i_{corr}) and anodic Tafel slopes (β_a) are obtained (**Table 1**). It can be observed that E_{corr} shifts towards more negative values as temperature increases, indicating that copper becomes more active and more prone to undergo corrosion at higher temperatures. Regarding i_{corr}, its value increases in general with temperature, since temperature favours the process of copper corrosion [43]. However, this tendency

8

is not valid at 100º C, since at this temperature i_{corr} values are lower than at 75º C for the 700 and 992 g/l LiBr solutions. This effect is related to the structural modifications that take place during the process of copper dissolution: as the temperature of the solution increases from 75º C to 100º C, the corrosion products formed on the electrode surface became more compact and less porous with temperature [43]. The value of the anodic Tafel slope, β_a, is approximately 60 mV, which is in accordance with the values obtained in bibliography for the apparent Tafel behaviour region [7, 12, 15, 24-27, 31].

Thermogalvanic corrosion

Open circuit measurements (ZRA)

Thermogalvanic corrosion between the cold and hot copper electrodes was evaluated by means of the ZRA technique, in the 400, 700 and 992 g/l LiBr solutions, imposing different temperature gradients (from 25 to 75 ºC in the 400 g/l LiBr solution and to 100º C in the rest of solutions). The mean values of thermogalvanic current densities (i_{thm}) and thermogalvanic potentials (E_{thm}), obtained for each hour of the test, are shown in **Figures 3 and 4**, respectively.

In the 400 g/l LiBr solution, the anodic member of the thermogalvanic pair is the hot copper electrode, since the i_{thm} values become negative as the temperature in the hot half-cell increases (**Figure 3a**). Moreover, the higher the temperature of the hot copper electrode, the more severe the thermogalvanic corrosion, since i_{thm} increases (in absolute value). Thermogalvanic current density also increases (in absolute value) with coupling time, indicating that corrosion products are not able to protect the copper surface against dissolution.

In the 700 g/l LiBr solution, the hot copper electrode is the anode of the thermogalvanic pair and the increase of temperature favours this anodic behaviour, since i_{thm} values increase with temperature (in absolute value) (**Figure 3b**) like in the 400 g/l LiBr solution. In the test performed at 25-50º C, the cold electrode is the anode during the first 3 hours of immersion, although a polarity reversal occurs after that due to the effect of temperature, speeding up the dissolution of the hot copper electrode. In the 25-75º C and 25-100º C tests, the anodic behaviour of the hot electrode is much more marked. It is worth noting that in the 25-75º C test, i_{thm} values are higher than at 25º-100º C during the first 3 hours of coupling. As it has been mentioned above, at 100º C the corrosion product layer formed on the hot electrode surface can undergo structural modification, becoming more compact due to its dehydration favoured by a temperature increase [43]. At the end of the tests, i_{thm} reaches more or less constant values, except at 25-100º C, where thermogalvanic current density keeps increasing with time (values of $|i_{thm}|$ higher than 130 µA cm^{-2}).

In the 992 g/l LiBr solution, the hot copper electrode is again the anode of the thermogalvanic pair and this behaviour is favoured when the hot half-cell temperature increases (**Figure 3c**), the same as in the other LiBr solution.

In general, E_{thm} values decrease with increasing temperature in all the LiBr solutions (**Figure 4**). According to Ashworth and Boden [17] a decrease of the thermogalvanic potential with temperature is indicative of a hot anode. Besides, thermogalvanic potential values remain approximately constant during the six hours of coupling,

indicating that no passive state is reached, since in passive systems the value of E_{thm} has been reported to decrease with immersion time [18].

It can be seen from **Figure 3** that i_{thm} values are rather high after the six hours of thermogalvanic coupling, especially in the tests performed at 25-75º C and 25-100º C. These values are expected to increase (in absolute value) with thermogalvanic coupling time or, at best, to reach a steady state, which evidences an active corrosion process, as opposed to the decrease of i_{thm} observed for passive systems [18]. This fact indicates that thermogalvanic corrosion of copper in LiBr solutions becomes more serious with coupling time, which could result in early system failure. Besides, thermogalvanic potential values are located in the region of apparent Tafel behaviour (**Figure 2**), where copper dissolution takes place according to eqs. (1) and (2), confirming the existence of an active corrosion process during thermogalvanic coupling.

Severity of thermogalvanic action

From **Figure 3**, thermogalvanic current density (i_{thm}) values of copper can be converted to an equivalent corrosion penetration rate using Faraday's equation. Thus, the rate of copper loss can be determined by:

$$\frac{dL}{dt} \equiv m = \frac{i_{thm} M}{nF\rho} \tag{8}$$

where m is the instantaneous corrosion rate of copper, i_{thm} is thermogalvanic current density (obtained at the end of the sixth hour of thermogalvanic coupling), M is the atomic weight of copper (63.55 g mol⁻¹), n is the number of equivalent exchanged electrons (1 according to eq. (1a)), F is Faraday's constant (96485.34 C mol⁻¹) and ρ is

copper density (8.94 g cm^{-3}). **Table 2** shows the estimations of corrosion rates for copper in the three LiBr solutions at the different imposed temperature gradients.

It can be seen in **Table 2** that corrosion rates of copper are significantly higher than 0.025 mm year^{-1} (which is generally regarded as the threshold of low corrosion rates and is related to passive systems) [45], especially in the 700 g/l LiBr solutions at 25ºC-75ºC and 25ºC-100ºC. Moreover, it can be noticed from **Figure 3** that in most cases, i_{thm} values tend to increase (in absolute value) with time even after 6 hours of immersion, without reaching a steady state. Thermogalvanic corrosion will remain as long as temperature differences exist in the system, which is the operating situation in heat exchangers, leading to their rapid deterioration. Hence, unlike in passive systems [18], thermogalvanic corrosion of copper in heavy brine LiBr solutions is severe and must be taken into account when designing heat exchangers in absorption plants.

Thermogalvanic potentials and Seebeck coefficient

The thermogalvanic potential, E_{th}, is the electromotive force of a non-isothermal or thermogalvanic cell, and is the result of four main effects [18, 46-48]: (a) electrode temperature, (b) thermal liquid junction potential (*TLJP*), (c) metallic thermocouple and (d) thermal diffusion gradient or Soret effect. In practical systems, (c) and (d) are often very small [46-50]. In neutral and alkaline solutions, (b) may be small [47]; moreover, *TLJP* can be effectively reduced to a small value by using the sintered glass membrane as a separator between hot and cold half-cells. Thus, the major contribution to the thermogalvanic potential is the difference in metal/solution Galvani potentials [18, 47].

The thermogalvanic potential can be expressed as follows:

$$E_{th} = \frac{\partial E_{th}}{\partial T} \cdot \Delta T + E_0 = E' \cdot \Delta T + E_0 \qquad (9)$$

where E_0 is the cell potential when there is no temperature gradient ($\Delta T = 0$). By analogy with thermoelectric phenomena, the gradient $\partial E_{th}/\partial T = E'$ is defined as the Seebeck coefficient [18, 51-53] and can be calculated from the slope of the linear representation E_{th} vs ΔT. Seebeck coefficients provide the sensitivity of the thermogalvanic cell emf (thermogalvanic potential) to a variation of the temperature gradient present in the system. Thus, the higher the value of the Seebeck coefficient (in absolute value), the smaller the variation in temperature gradient required to generate large potential differences between the electrodes, and the more prone the metal to undergo thermogalvanic corrosion.

Figure 5 shows the results of the experiments that evaluate the concentration dependence of the Seebeck coefficient for copper in the three LiBr solutions under study. The graphs show typical experimental measurements of Seebeck coefficients in thermogalvanic cells, since a linear relation is observed for all concentrations [18, 19, 48, 50, 54, 55]. Seebeck coefficients are negative for all the LiBr solutions, meaning that the electric potential of the cold electrode is positive with respect to the hot one. Therefore, electrons diffuse from the hot zone to the cold zone and the hot electrode is the anode of the thermogalvanic pair [19, 50, 52], in agreement with the ZRA results for i_{thm}.

The similar slopes in **Figure 5** indicate that the Seebeck coefficient does not depend on the LiBr concentration and remains approximately constant. This fact can be explained in terms of LiBr concentrations, higher than 31 wt.%. Other authors [18, 48, 50] have found that in several solutions ($CuSO_4$ and LiBr) whose concentrations were higher than 6.4 wt.%, the value of Seebeck coefficient did not depend on the electrolyte concentration.

EIS measurements

EIS spectra

By way of illustration, **Figure 6** shows the evolution of the impedance response of the cold and hot copper electrodes immersed in 700 g/l LiBr solution before and after the thermogalvanic coupling (BTC and ATC, respectively), in the form of Nyquist and Bode-phase plots. Three time constants can be discerned in the Bode plots, as it has been reported in numerous studies concerning copper behaviour against corrosion in halide solutions [56-59]. At high frequencies, the phase angle drops to 0 degrees as frequency increases; this response is typical of resistive behaviour and corresponds to the electrolyte resistance. At intermediate frequencies, the Bode plots show two phase maxima close to 45 degrees, which is characteristic of diffusion processes [29, 58]. In the low frequency region, phase angle values do not decrease with decreasing frequencies, but remain constant or even increase slightly.

In the Nyquist plots, a semicircle in the high frequency region is followed by a diffusion tail in the intermediate and low frequency region, characteristic of Warburg impedance

14

behaviour related to diffusion processes (enlarged plots in **Figure 6**). This implies that copper corrosion in LiBr solutions can be diffusion controlled, which is in accordance with reactions (1) and (2) taking place within the region of apparent Tafel behaviour (**Figure 2**). This mass transfer process is the diffusion of the soluble complex $CuBr_2^-$ framed in the process of copper active corrosion.

The first time constant observed at high-intermediate frequencies (≈ 1 kHz) in **Figure 6** corresponds to a maximum phase angle and is related to charge transfer processes. Before thermogalvanic coupling, e cold electrodes have higher phase angles in this region than the hot electrodes. After thermogalvanic coupling, both electrodes reach higher phase angle values than before coupling, evidencing that the resistance to charge transfer is somewhat increased after 6 hours of thermogalvanic coupling. The second time constant observed at low-intermediate frequencies ($\approx 1\text{-}10$ Hz) in the Bode-phase diagrams of **Figure 6** is related to the corrosion products formed on the copper surface. In general, the anode of the thermogalvanic pair (the hot electrode) has higher phase angle values than the cathode (the cold electrode), indicating a slightly better capacitive behaviour of the hot electrode after coupling. Nevertheless, these phase angle values are rather low, and the layer of corrosion products cannot be regarded as an insulator, since it offers little protection to the electrode. It can be noticed from the Nyquist plots in **Figure 6** that before thermogalvanic coupling the cold electrode has the best resistive behaviour. In general, the resistive behaviour of the hot electrode (the anode of the pair) improves after thermogalvanic coupling (with the exception of the 25-100º C test), whereas the resistive behaviour of the cold electrode (the cathode of the pair) gets worse with coupling time.

Electrical equivalent circuit

The EIS spectra of the cold and hot copper electrodes immersed in the three LiBr solutions before and after thermogalvanic coupling have been analysed by fitting the data to the electrical equivalent circuit shown in **Figure 7**, which has been used elsewhere to model the copper/electrolyte interface in the presence of chlorides [27, 30, 36, 56, 58, 60-62]. In this equivalent circuit, R_S represents the electrolyte resistance. CPE_1 is the electrical double layer capacitance which behaves as a non-ideal capacitor. This double layer capacitance is connected in parallel to the Faradaic impedace, which is composed of a charge transfer resistance (R_1) corresponding to the CuBr and $CuBr_2^-$ formation reactions, eqs. (1a) and (1b), the capacitance and resistance of the layer of corrosion products formed on the copper surface (CPE_2 *and* R_2, respectively) and a finite Warburg impedance or OFLD element (Open Boundary Finite Length Diffusion Model). The OFLD element is used to take into account diffusion processes with finite diffusion layer, assuming that the Nernst diffusion layer thickness is comparable to the distance travelled by diffusing species. In the present case, diffusion occurs due to the partial obstruction of mass transfer by the corrosion product layer formed on the electrode surface (mainly CuBr, eq. (1a)). Hence, as it has been explained above, the copper corrosion mechanism in LiBr solutions is not only charge-transfer controlled but also mass-transfer controlled due to the diffusion of the soluble complex $CuBr_2^-$.

A CPE (Constant Phase Element) represents a deviation from the ideal behaviour of a capacitor and can be used to replace a conventional capacitance. CPEs are used to model surface heterogeneities, roughness effects and variations in properties and/or

composition of surface layers [26, 60, 63, 64]. The impedance of a constant-phase element is defined as:

$$Q = Z_{CPE} = \left[C(j\omega)^\alpha\right]^{-1} \tag{10}$$

where α is the CPE power and accounts for deviation from ideality of capacitive behaviour. Thus, for a perfectly polished surface without heterogeneities, the CPE power yields a value of $\alpha = 1$ and represents an ideal capacitor. For real electrodes, $\alpha < 1$. When there are diffusion processes, α is close to 0.5.

The equation of the OFLD element used to model $CuBr_2^-$ diffusion through the corrosion product layer is:

$$Z_W(OFLD) = \frac{\tanh\left(B \cdot \sqrt{j\omega}\right)}{Y_0 \cdot \sqrt{j\omega}} \tag{11}$$

where $B = l / (D)^{1/2}$, D is the diffusion coefficient, l is the diffusion layer thickness, $Y_0 = (\sigma(2)^{1/2})^{-1}$ and σ is the Warburg coefficient. Since the Warburg coefficient is inversely proportional to the admittance Y_0, the higher this coefficient the higher the mass-transfer resistance. Therefore, from the parameters B and Y_0, the diffusion layer thickness l, which can be regarded as equivalent to the corrosion products layer thickness, and the Warburg coefficient can be calculated.

The diffusion coefficient of the $CuBr_2^-$ complex has been calculated from the diffusion coefficient of Br^- in the different LiBr solutions at the different temperatures, supposing that $D_{Br^-} \approx 4D_{CuBr_2^-}$ as Deslouis *et. at.* did for $CuCl_2^-$ [65]. The values of D_{Br^-} in the different LiBr solutions at the different temperatures have been calculated from data for LiBr solutions at 25º C [66], using the Stokes-Einstein equation for diffusivity. This equation is derived from continuum fluid mechanics and classical thermodynamics for the motion of large spherical particles in a liquid. The Stokes-Einstein equation is [67]:

$$D_{AB} = \frac{kT}{6\pi\, r_A \mu_B} \qquad (12)$$

where A refers to the solute and B refers to the solvent, D is the diffusion coefficient, k is Boltzman Constant ($1.38 \cdot 10^{-23}$ J/K), μ is the dynamic viscosity of the pure solvent (in Pa·s), T is the temperature and r is the solute molecule radius. Since k and r_A do not vary with temperature, an approximate dependence of the diffusion coefficient on temperature in liquids can be found by using the following expression derived from Stokes-Einstein equation:

$$\frac{D_{T1}}{D_{T2}} = \frac{T_1}{T_2}\frac{\mu_{T2}}{\mu_{T1}} \qquad (13)$$

Viscosity values of pure water at different temperatures have been determined from bibliographic data [66]. Diffusivities of $CuBr_2^-$ in the LiBr solutions at different temperatures are in the range of $5 \cdot 10^{-6} - 3 \cdot 10^{-5}$ cm s^{-2}. These values are of the same order of magnitude as the diffusion coefficient for $CuCl_2^-$ species in 1 M HCl at 25º C [62].

The stability of the system is crucial for the validity of EIS measurements. In order to validate the EIS data and examine the system with respect to the linearity, causality and stability, the Kramers–Kronig transforms have been applied to the experimental impedance data by transforming the real axis into the imaginary axis and the imaginary axis into the real axis and then comparing the transformed quantities with the respective experimental data. Only those experimental data satisfying the four physical conditions of causality, stability, linearity, and finiteness, can be used to describe the properties of the systems in terms of LST (Linear Systems Theory) and hence linear models. **Figure 8** has been obtained for the test 25-75º C in the 992 g/l LiBr solution, where the system seems not to be stable (see E_{th} values in **Figure 4c**). This figure shows good agreement between the set of the impedance data and corresponding K–K transforms, demonstrating that the system satisfies the constraints of LST and is therefore stable.

The equivalent circuit parameters calculated for the cold and hot copper electrodes before and after thermogalvanic coupling (BTC and ATC, respectively) in the different LiBr solutions are presented in **Tables 3-5**. The chi-square values, χ^2, are on the order of 10^{-3}-10^{-4}, which indicates the goodness of fit of the equivalent circuit used in this work. The values of the charge transfer resistance, R_1, decrease with increasing temperatures and increase with coupling time, meaning that temperature favours charge transfer on the electrodes surface, while immersion time makes charge transfer somewhat difficult. Nevertheless, electrode polarity seems to have no noticeable effect on this parameter, since the tendency of the anode and cathode of the thermogalvanic pair is similar. It can also be noticed that R_1 values are rather small and close to the electrolyte resistance, R_S, implying that the charge transfer process of copper electrodissolution takes place spontaneously and actively. The values of the double layer capacitance, C_1, are

consistent with observations for double layer capacities at the metal/electrolyte interface, typically in the range of 10 to 40 $\mu F/cm^2$ [68, 69]. C_1 values do not show a clear tendency with temperature, coupling time or electrode polarity. CPE power values for the first capacitance, α_1, are slightly lower than unity, indicating that the behaviour of the electrical double layer corresponds to a capacitor with some imperfections.

The second time constant, represented by ($R_2//CPE_2$) in **Figure 7** has been related to the surface layer formed by corrosion products (mainly CuBr according to eqs. (1a) and (3)). The resistance of this layer, R_2, is higher than the charge transfer resistance, R_1, taking values from 60 to 500 Ω cm^2. However, R_2 values are rather low compared with those obtained for passive films formed on austenitic stainless steels in the same heavy brine LiBr solutions, whose order of magnitude is hundreds of $k\Omega$ cm^2 [18]. As shown in **Tables 3-5**, R_2 tend to decrease with increasing temperature before thermogalvanic coupling, indicating a worse corrosion behaviour of copper at higher temperatures. By contrast, with coupling time, R_2 tends to increase in the anode of the pair (the hot electrode) and tends to decrease in the cathode (the cold electrode). This fact can be related to the thickness of the surface layer, since this layer tends to grow as copper electrodissolution progresses in the anode, whereas it grows to a lesser extent on the cathode surface where it can be further electrochemically reduced during thermogalvanic coupling. The polarisation resistance, R_P, has been calculated as $R_1 + R_2$, and represents the total resistance of charge transfer processes, whereas diffusion is modelled by the Warburg component. Since the main contribution to R_p is the layer of corrosion products, its tendency with temperature and coupling time is the same as R_2. The values of the surface layer capacitance, C_2, are very high, of the order of $10^{-3} - 10^{-2}$ F cm^{-2}, indicating that the layer has no insulating properties. Moreover, α_2 values

deviate greatly from 1, indicating severe surface heterogeneity and a very porous nature. Values of α_2 close to 0.5 evidence the presence of a diffusion process, supporting the use of a finite-length Warburg element (OFLD) to model mass transfer phenomena. Hence, the relatively low values of R_2 and the high values of C_2 verify the high defectiveness and the low protective properties of the CuBr layer.

The corrosion product layer thickness, δ, and the Warburg coefficient, σ, have been calculated from the parameters of the OFLD model. In general, thickness increases with thermogalvanic coupling time in the anode of the pair (hot electrode) and decreases in the cathode (cold electrode). These results are in accordance with the R_2 values and suggest that the formation of a CuBr layer through the active electrodissolution of copper, eqs. (1a) and (3), takes place predominantly on the anode surface, while reduction processes take place primarily on the cathode surface. In some cases, the thickness of the surface layer also increases in the cathode after thermogalvanic coupling. The polarity of the electrodes is determined by the predominant behaviour as anode or as cathode; hence, the cathode of the pair could undergo some degree of dissolution, which is reflected by the formation of a corrosion product layer. As for the Warburg coefficient, σ, its value decreases with temperature, indicating a decrease in mass transfer resistance at higher temperatures, except for the 992 g/l LiBr solution. No effect of electrode polarity on the Warburg coefficient can be noticed from **Tables 3-5**.

Conclusions

Potentiodynamic polarisation curves for copper in heavy brine LiBr solutions exhibit different anodic regions: (1) *apparent Tafel behaviour region*, where the formation of CuBr and $CuBr_2^-$ species occurs by a two-stage process which is controlled both by the electrodissolution process and the diffusion of complex $CuBr_2^-$ species; (2) *: maximum and limit current density region*, where the formation and growth of a porous and very insoluble CuBr layer takes place; and (3) *high potential region,* where the CuBr layer dissolves and Cu(II) species such as CuO are formed.

From the potentiodynamic polarisation curves, it can be said that temperature negatively affects the corrosion behaviour of copper in heavy brine LiBr solutions, since E_{corr} shifts towards more negative values and current density values increase with increasing temperature.

The anodic member of the thermogalvanic pair is the hot copper electrode in the three LiBr solutions under study. Moreover, temperature enhances the anodic behaviour of the hot copper electrodes. Rates of copper loss are by far higher than 0.025 mm year^{-1}, which is regarded as the threshold of low corrosion rates. Moreover, thermogalvanic current density values also increase (in absolute value) with coupling time, without reaching a steady state, leading to rapid deterioration of process equipment. Thus, it can be said that thermogalvanic corrosion of copper in heavy brine LiBr solutions is severe and must be taken into account when designing heat exchangers in absorption plants.

Seebeck coefficients are negative for all the LiBr solutions, meaning that the electrons diffuse from the hot zone to the cold zone and the hot electrode is the anode of the thermogalvanic pair, in agreement with the ZRA results for i_{thm}.

The EIS plots show three time constants, related to charge transfer on the electrode surface, the properties of the CuBr layer and the diffusion of the soluble $CuBr_2^-$ complex, respectively. The charge transfer process responsible for the formation of CuBr and $CuBr_2^-$ is enhanced by temperature, although it is not affected by electrode polarity. The thickness (δ_{CuBr}) and the resistance (R_2) of the corrosion product layer increase on the anode surface after thermogalvanic coupling, whereas R_2 and δ_{CuBr} decrease on the cathode surface.

ACKNOWLEDGEMENTS

REFERENCES

[1] S. C. Kaushik, A. Arora, Energy and exergy analysis of single effect and series flow double effect water-lithium bromide absorption refrigeration systems, Int. J. Refrig. 32 (2009) 1247-1258.

[2] O. Kaynakli, M. Kilic, Theoretical study on the effect of operating conditions on performance of absorption refrigeration system, Energ. Convers. Manage. 48 (2007) 599-607.

[3] R. D. Misra, P. K. Sahoo, A. Gupta, Thermoeconomic evaluation and optimization of a double-effect H2O/LiBr vapour-absorption refrigeration system, Int. J. Refrig. 28 (2005) 331-343.

[4] P. Srikhirin, S. Aphornratana, S. Chungpaibulpatana, A review of absorption refrigeration technologies, Renew. Sust. Energ. Rev. 5 (2001) 343-372.

[5] G. A. Florides, S. A. Kalogirou, S. A. Tassou, L. C. Wrobel, Design and construction of a LiBr-water absorption machine, Energ. Convers. Manage. 44 (2003) 2483-2508.

[6] H. Cheng, Cu(II) Removal from lithium bromide refrigerant by chemical precipitation and electrocoagulation, Sep. Purif. Technol. 52 (2006) 191-195.

[7] M. Itagaki, Y. Hirata, K. Watanabe, Anodic dissolution and disproportional reaction of copper in bromide solution investigated by channel flow electrode, Corros. Sci. 45 (2003) 1023-1036.

[8] A. Igual-Muñoz, J. García-Antón, J. L. Guiñón, V. Pérez-Herranz, Galvanic Studies of Copper Coupled to Alloy 33 and Titanium in Lithium Bromide Solutions, CORROSION 58 (2002) 995-1003.

[9] A. Igual-Muñoz, J. García-Antón, J. L. Guiñón, V. Pérez-Herranz, Comparison of inorganic inhibitors of copper, nickel and copper-nickels in aqueous lithium bromide solution, Electrochim. Acta 50 (2004) 957-966.

[10] P. J. Boden, Corrosion of Cu and Cu-base alloys under conditions of boiling heat transfer--I. Corrosion of Cu, Corros. Sci. 11 (1971) 353-362.

[11] G. E. C. Bell, M. J. Schiff, D. F. Wilson, Field Observations and Laboratory Investigations of Thermogalvanic Corrosion of Copper Tubing, Corrosion 97, Paper No. 568. 1997. Houston, TX, NACE International.

[12] T. Aben, D. Tromans, Anodic Polarization Behavior of Copper in Aqueous Bromide and Bromide/Benzotriazole Solutions, J. Electrochem. Soc. 142 (1995) 398-404.

[13] D. Itzhak, T. Greenberg, Galvanic Corrosion of a Copper Alloy in Lithium Bromide Heavy Brine Environments, CORROSION 55 (1999) 795-799.

[14] A. Igual-Muñoz, J. García-Antón, J. L. Guiñón, V. Pérez-Herranz, Galvanic Study of Zinc and Copper in Lithium Bromide Slutions at Different Temperatures, CORROSION 57 (2001) 516-522.

[15] M. J. Muñoz-Portero, J. García-Antón, J. L. Guiñón, V. Pérez-Herranz, Anodic Polarization Behavior of Copper in Concentrated Aqueous Lithium Bromide Solutions and Comparison with Pourbaix Diagrams, CORROSION 61 (2005) 464-472.

[16] R. Sánchez-Tovar, M. T. Montañés, J. García-Antón, The effect of temperature on the galvanic corrosion of the copper/AISI 304 pair in LiBr solutions under hydrodynamic conditions, Corros. Sci. 52 (2010) 722-733.

[17] V. Ashworth, P. J. Boden, The thermogalvanic corrosion of mild steel in alkaline solution I: Actively dissolving electrodes, Corros. Sci. 14 (1974) 183-197.

[18] R. M. Fernández-Domene, E. Blasco-Tamarit, D. M. García-García, J. García-Antón, Thermogalvanic corrosion of Alloy 31 in different heavy brine LiBr solutions, Corros. Sci. 55 (2012) 40-53.

[19] J. W. Tester. Evaluation of Thermogalvanic Cells for the Conversion of Heat to Electricity, MIT Energy Lab, Technical Report MIT-EL, 92-007 (1992).

[20] R. Hu, B. A. Cola, N. Haram, J. N. Barisci, S. Lee, S. Stoughton, G. Wallace, C. Too, M. Thomas, A. Gestos, M. E. d. Cruz, J. P. Ferraris, A. A. Zakhidov, R. H. Baughman, Harvesting Waste Thermal Energy Using a Carbon-Nanotube-Based Thermo-Electrochemical Cell, Nano Lett. 10 (2010) 838-846.

[21] J. C. Verhoef, E. Barendrecht, Electrochemical behaviour of iodide at a rotating platinum disk electrode in methanol, Electrochim. Acta 23 (1978) 433-438.

[22] V. S. Bagotsky, Fundamentals of Electrochemistry, 2nd ed., John Wiley & Sons, Hoboken, NJ, 2006, Ch. 5.

[23] D. Tromans, J. C. Silva, Behavior of Copper in Acidic Sulfate Solution: Comparison with Acidic Chloride, CORROSION 53 (1997) 171-178.

[24] H. P. Lee, K. Nobe, Kinetics and Mechanisms of Cu Electrodissolution in Chloride Media, J. Electrochem. Soc. 133 (1986) 2035-2043.

[25] F. K. Crundwell, The anodic dissolution of 90% copper-10% nickel alloy in hydrochloric acid solutions, Electrochim. Acta 36 (1991) 2135-2141.

[26] A. V. Benedeti, P. T. A. Sumodjo, K. Nobe, P. L. Cabot, W. G. Proud, Electrochemical studies of copper, copper-aluminium and copper-aluminium-silver alloys: Impedance results in 0.5M NaCl, Electrochim. Acta 40 (1995) 2657-2668.

[27] H. Y. Ma, C. Yang, S. H. Chen, Y. L. Jiao, S. X. Huang, D. G. Li, J. L. Luo, Electrochemical investigation of dynamic interfacial processes at 1-octadecanethiol-modified copper electrodes in halide-containing solutions, Electrochim. Acta 48 (2003) 4277-4289.

[28] E. S. Sherif, R. M. Erasmus, J. D. Comins, Effects of 3-amino-1,2,4-triazole on the inhibition of copper corrosion in acidic chloride solutions, J. Colloid Interf. Sci. 311 (2007) 144-151.

[29] D. Q. Zhang, L. X. Gao, G. D. Zhou, Inhibition of copper corrosion by bis-(1-benzotriazolymethylene)-(2,5-thiadiazoly)-disulfide in chloride media, Appl. Surf. Sci. 225 (2004) 287-293.

[30] K. F. Khaled, Studies of the corrosion inhibition of copper in sodium chloride solutions using chemical and electrochemical measurements, Mat. Chem. Phys. 125 (2011) 427-433.

[31] Y. G. Chun, S. I. Pyun, C. H. Kim, Effect of aluminium content on the anodic behaviour of copper-aluminium alloys in 3.5 wt% NaCl solution, Mater. Lett. 20 (1994) 265-270.

[32] W. Li, L. Hu, S. Zhang, B. Hou, Effects of two fungicides on the corrosion resistance of copper in 3.5% NaCl solution under various conditions, Corros. Sci. 53 (2011) 735-745.

[33] L. Brossard, Potentiodynamic Investigation of Copper in the Presence of Bromide Ions, J. Electrochem. Soc. 131 (1984) 1847-1849.

[34] J. Y. Josefowicz, L. Xie, G. C. Farrington, Observation of Intermediate CuCl Species during the Anodic Dissolution of Cu Using Atomic Force Microscopy, J. Phys. Chem. 97 (1993) 11995-11998.

[35] O. E. Barcia, O. R. Mattos, N. Pebere, B. Tribollet, Mass-Transport Study for the Electrodissolution of Copper in 1M Hydrochloric Acid Solution by Impedance, J. Electrochem. Soc. 140 (1993) 2825-2832.

[36] E. M. Sherif, S. M. Park, Inhibition of copper corrosion in acidic pickling solutions by N-phenyl-1,4-phenylenediamine, Electrochim. Acta 51 (2006) 4665-4673.

[37] H. Otmacic, E. Stupnisek-Lisac, Copper corrosion inhibitors in near neutral media, Electrochim. Acta 48 (2003) 985-991.

[38] G. Kear, B. D. Barker, F. C. Walsh, Electrochemical corrosion of unalloyed copper in chloride media--a critical review, Corros. Sci. 46 (2004) 109-135.

[39] R. Vera, F. Bastidas, M. Villarroel, A. Oliva, A. Molinari, D. Ramírez, R. del Río, Corrosion inhibition of copper in chloride media by 1,5-bis(4-dithiocarboxylate-1-dodecyl-5-hydroxy-3-methylpyrazolyl)pentane, Corros. Sci. 50 (2008) 729-736.

[40] S. M. Milic, M. M. Antonijevic, Some aspects of copper corrosion in presence of benzotriazole and chloride ions, Corros. Sci. 51 (2009) 28-34.

[41] H. Otmacic Curkovic, E. Stupnisek-Lisac, H. Takenouti, The influence of pH value on the efficiency of imidazole based corrosion inhibitors of copper, Corros. Sci. 52 (2010) 398-405.

[42] G. Kear, B. D. Barker, K. Stokes, F. C. Walsh, Electrochemical Corrosion Behaviour of 90-10 Cu-Ni Alloy in Chloride-Based Electrolytes, J. Appl. Electrochem. 34 (2004) 659-669.

[43] M. J. Muñoz-Portero, J. García-Antón, J. L. Guiñón, V. Pérez-Herranz, Corrosion of Copper in Aqueous Lithium Bromide Concentrated Solutions by Immersion Testing, CORROSION 62 (2006) 1018-1027.

[44] M. M. Antonijevic, S. M. Milic, M. B. Petrovic, Films formed on copper surface in chloride media in the presence of azoles, Corros. Sci. 51 (2009) 1228-1237.

[45] J. R. Scully and R. G. Kelly in: S. D. Cramer (Ed.), B. S. Covino, Jr. (Ed.), Corrosion: Fundamentals, Testing and Protection, Vol. 13, ASM Handbook, ASM International, 2003.

[46] L. B. Kriksunov. Thermogalvanic Effects in Corrosion in Supercritical Water, Corrosion 98, NACE, Houston, TX, 1998, paper no. 418.

[47] P.J. Boden in: L.L. Shreir (Ed.), R.A. Jarman (Ed.), G.T. Burstein (Ed.), Corrosion and Corrosion Control, vol. 1, 3rd ed., Butterworth-Heinemann, Oxford, 1994.

[48] K. Szabó, E. Földesi, Study of the CuCu(NO3)2·H2OCu electrochemical thermocouple at low temperatures, J. Electroanal. Chem. 452 (1998) 107-111.

[49] B. E. Conway, D. P. Wilkinson, Non-isothermal cell potentials and evaluation of entropies of ions and of activation for single electrode processes in non-aqueous media, Electrochim. Acta 38 (1993) 997-1013.

[50] U. B. Holeschovsky, Analysis of flooded flow fuel cells and thermogalvanic generators, Ph.D. Thesis, Massachusetts Institute of Technology (1994).

[51] D.D. Pollock in: D.M. Rowe (Ed.), CRC Handbook of Thermoelectrics, 1st ed., CRC Press, Boca Ratón, FL, 1995, Ch. 2.

[52] S.O. Kasap, Thermoelectric effects in metals: thermocouples, An e-booklet, 2001, http://materials.usask.ca/samples/Thermoelectric-Seebeck.pdf (22-03-2011).

[53] J. Newman, Thermoelectric Effects in Electrochemical Systems, Ind. Eng. Chem. Res. 34 (1995) 3208-3216.

[54] D. S. Carr, C. F. Bonilla, Thermogalvanic Potentials II. Nickel in Neutral Sulfate Solution, J. Electrochem. Soc. 99 (1952) 475-482.

[55] R. Schneebaum, B. R. Sundheim, Thermoelectric Properties of the Silver Nitrate+Sodium Nitrate System, Discuss. Faraday Soc. 32 (1961) 197-202.

[56] E. S. Sherif, R. M. Erasmus, J. D. Comins, Inhibition of copper corrosion in acidic chloride pickling solutions by 5-(3-aminophenyl)-tetrazole as a corrosion inhibitor, Corros. Sci. 50 (2008) 3439-3445.

[57] Y. Van Ingelgem, A. Hubin, J. Vereecken, Investigation of the first stages of the localized corrosion of pure copper combining EIS, FE-SEM and FE-AES, Electrochim. Acta 52 (2007) 7642-7650.

[58] R. M. El-Sherif, K. M. Ismail, W. A. Badawy, Effect of Zn and Pb as alloying elements on the electrochemical behavior of brass in NaCl solutions, Electrochim. Acta 49 (2004) 5139-5150.

[59] Y. Van Ingelgem, E. Tourwé, J. Vereecken, A. Hubin. Application of multisine impedance spectroscopy, FE-AES and FE-SEM to study the early stages of copper corrosion, Electrochim. Acta 53 (2008) 7523-7530.

[60] K. M. Ismail, A. M. Fathi, W. A. Badawy, Electrochemical behavior of copper-nickel alloys in acidic chloride solutions, Corros. Sci. 48 (2006) 1912-1925.

[61] W. A. Badawy, K. M. Ismail, A. M. Fathi, Effect of Ni content on the corrosion behavior of Cu-Ni alloys in neutral chloride solutions, Electrochim. Acta 50 (2005) 3603-3608.

[62] J. P. Diard, J. M. Le Canut, B. Le Gorrec, C. Montella, Copper electrodissolution in 1M HCl at low current densities II. Electrochemical impedance spectroscopy study, Electrochim. Acta 43 (1998) 2485-2501.

[63] A. Nagiub, F. Mansfeld, Evaluation of corrosion inhibition of brass in chloride media using EIS and ENA, Corros. Sci. 43 (2001) 2147-2171.

[64] T. Kosec, D. K. Merl, I. Milosev, Impedance and XPS study of benzotriazole films formed on copper, copper-zinc alloys and zinc in chloride solution, Corros. Sci. 50 (2008) 1987-1997.

[65] C. Deslouis, O. R. Mattos, M. M. Musiani, B. Tribollet, Comments on mechanisms of copper electrodissolution in chloride media, Electrochim. Acta 38 (1993) 2781-2783.

[66] D.R.Lide (Ed.), CRC Handbook of Chemistry and Physics, CRC Press, Boca Raton, FL, 2008.

[67] R. B. Bird, W. E. Stewart, and E. N. Lightfoot, Transport Phenomena, John Wiley & Sons, New York, NY, 2002.

[68] A. J. Bard and L. R. Faulkner, Electrochemical Methods: Fundamentals and Applications, John Wiley & Sons, New York, NY, 2001.

[69] M. E. Orazem and B. Tribollet, Electrochemical Impedance Spectroscopy, John Wiley & Sons, Hoboken, NJ, 2008.

Tables captions

Table 1.

Values of E_{corr} and i_{corr} for copper in 400, 700 and 992 g/l LiBr solutions at 25, 50, 75 and 100º C.

Table 2.

Rates of copper loss in 400, 700 and 992 g/l LiBr solutions at different temperatures, in presence of thermogalvanic coupling (by i_{thm}).

Table 3.

Calculated equivalent circuit parameters for cold and hot copper electrodes before and after the thermogalvanic coupling (BTC and ATC, respectively) in the 400 g/l LiBr solution.

Table 4.

Calculated equivalent circuit parameters for cold and hot copper electrodes before and after the thermogalvanic coupling (BTC and ATC, respectively) in the 700 g/l LiBr solution.

Table 5.

Calculated equivalent circuit parameters for cold and hot copper electrodes before and after the thermogalvanic coupling (BTC and ATC, respectively) in the 992 g/l LiBr solution.

Figures captions

Fig. 1.

Electrochemical cell used for thermogalvanic corrosion tests.

Fig. 2.

Potentiodynamic polarisation curves for copper in the 700 g/l LiBr solution at 25, 50, 75 and 100º C.

Fig. 3.

Mean values of thermogalvanic current density registered between the pair cold copper – hot copper during each hour of the test at different imposed temperature gradients in the (a) 400 g l^{-1} LiBr, (b) 700 g l^{-1} LiBr and (c) 992 g l^{-1} LiBr solutions.

Fig. 4.

Mean values of thermogalvanic potential registered between the pair cold copper – hot copper during each hour of the test at different imposed temperature gradients in the (a) 400 g l^{-1} LiBr, (b) 700 g l^{-1} LiBr and (c) 992 g l^{-1} LiBr solutions.

Fig. 5.

Thermogalvanic potential (E_{th}) vs. temperature gradient (ΔT) for the three LiBr solutions under study.

Fig. 6.

Nyquist and Bode-phase plots for the pair cold copper – hot copper at OCP in the 700 g l^{-1} LiBr solution at the temperature gradients of (a) 25ºC-25ºC, (b) 25ºC-50ºC, (c) 25ºC-75ºC and (d) 25ºC-100ºC, before and after the thermogalvanic coupling (BTC and ATC, respectively).

Fig. 7.

Representation of the equivalent circuit proposed for the interpretation of EIS spectra of copper in the LiBr solutions under study.

Fig. 8.

Kramers–Kronig transforms of EIS data for the hot copper electrode after thermogalvanic coupling in the 992 g/l LiBr solution.

Table 1

C_{LiBr}/g l^{-1}	T/°C	E_{corr} vs (Ag/AgCl)/mV	i_{corr}/μA cm^{-2}	β_a/mV
400	25	-339 ± 21	10.36 ± 2.62	61.5
	50	-345 ± 5	19.63 ± 3.12	60.6
	75	-450 ± 16	37.16 ± 0.35	61.7
700	25	-399 ± 6	21.02 ± 7.85	63.3
	50	-407 ± 4	28.87 ± 6.33	62.4
	75	-424 ± 11	50.78 ± 3.31	62.8
	100	-492 ± 9	36.16 ± 4.22	61.5
992	25	-481 ± 11	13.36 ± 3.29	61.9
	50	-463 ± 17	29.84 ± 0.20	54.9
	75	-490 ± 5	36.71 ± 2.10	59.6
	100	-519 ± 9	31.01 ± 2.07	61.2

C_{LiBr}/g l^{-1}	T/°C	E_{corr} vs (Ag/AgCl)/mV	i_{corr}/μA cm^{-2}	β_a/mV

Table 2

$C_{LiBr}/g\ l^{-1}$	Test	$|i_{thm}|/\mu A\ cm^{-2}$	$m_{ithm}/mm\ year^{-1}$
400	25ºC-50ºC	13.05	0.303
	25ºC-75ºC	23.89	0.555
700	25ºC-50ºC	11.62	0.270
	25ºC-75ºC	55.98	1.301
	25ºC-100ºC	139.26	3.236
992	25ºC-50ºC	3.74	0.087
	25ºC-75ºC	8.91	0.207
	25ºC-100ºC	20.49	0.476

Table 3

Electrode	$R_S/\Omega\ \text{cm}^2$	$R_1/\Omega\ \text{cm}^2$	$C_1/\text{F cm}^{-2}$	α_1	$R_2/\Omega\ \text{cm}^2$	$R_P/\Omega\ \text{cm}^2$	$C_2/\text{F cm}^{-2}$	α_2	$\delta/\mu\text{m}$	$\sigma/\Omega\ \text{cm}^2\,\text{s}^{-1/2}$	χ^2
25ºC-25ºC											
Cold and hot (BTC)	1.13	22.48	$2.34\cdot10^{-5}$	0.91	527.91	550.39	0.003	0.49	124	192	$5.8\cdot10^{-4}$
Cold (ATC)	1.20	13.01	$1.38\cdot10^{-5}$	0.85	252.25	265.26	0.001	0.56	134	70	$7.0\cdot10^{-4}$
Hot (ATC)	1.10	13.22	$2.15\cdot10^{-5}$	0.87	589.95	603.17	0.003	0.52	98	139	$7.0\cdot10^{-4}$
25ºC-50ºC											
Cold (BTC)	1.13	22.48	$2.34\cdot10^{-5}$	0.91	527.91	550.39	0.003	0.49	124	192	$5.8\cdot10^{-4}$
Hot (BTC)	0.90	2.18	$1.62\cdot10^{-5}$	0.93	155.82	158.00	0.004	0.40	112	17	$9.9\cdot10^{-4}$
Cold (ATC)	1.13	21.94	$3.54\cdot10^{-5}$	0.88	577.87	599.81	0.002	0.47	89	479	$2.5\cdot10^{-3}$
Hot (ATC)	0.97	17.75	$2.67\cdot10^{-5}$	0.82	168.90	186.65	$3\cdot10^{-4}$	0.50	255	67	$2.7\cdot10^{-3}$
25ºC-75ºC											
Cold (BTC)	1.13	22.48	$2.34\cdot10^{-5}$	0.91	527.91	550.39	0.003	0.49	124	192	$5.8\cdot10^{-4}$
Hot (BTC)	0.68	0.76	$2.69\cdot10^{-5}$	0.98	249.50	250.26	0.067	0.44	111	140	$1.1\cdot10^{-3}$
Cold (ATC)	1.09	32.48	$2.79\cdot10^{-5}$	0.91	397.95	430.43	0.001	0.51	113	64	$8.7\cdot10^{-4}$
Hot (ATC)	0.67	2.18	$1.96\cdot10^{-5}$	0.98	168.40	170.58	0.038	0.41	134	191	$5.9\cdot10^{-4}$

Table 4

Electrode	R_S/Ω cm^2	R_1/Ω cm^2	C_1/F cm^{-2}	α_1	R_2/Ω cm^2	R_P/Ω cm^2	C_2/F cm^{-2}	α_2	δ/μm	σ/Ω cm^2 s$^{-1/2}$	χ^2
25ºC-25ºC											
Cold and hot (BTC)	1.32	7.14	2.64·10^{-5}	0.88	506.87	514.01	0.024	0.48	139	145	6.3·10^{-4}
Cold (ATC)	1.42	16.49	2.33·10^{-5}	0.91	346.50	362.99	0.003	0.47	147	46	8.2·10^{-4}
Hot (ATC)	1.32	24.37	2.50·10^{-5}	0.89	265.20	289.57	0.002	0.50	173	29	8.5·10^{-4}
25ºC-50ºC											
Cold (BTC)	1.32	7.14	2.64·10^{-5}	0.88	506.87	514.01	0.024	0.48	139	145	6.3·10^{-4}
Hot (BTC)	0.99	0.41	2.18·10^{-5}	0.98	67.82	68.23	0.028	0.42	171	42	6.1·10^{-4}
Cold (ATC)	1.23	19.32	2.69·10^{-5}	0.87	180.00	199.32	0.001	0.53	202	30	1.1·10^{-3}
Hot (ATC)	0.98	8.36	2.10·10^{-5}	0.94	449.00	457.36	0.069	0.39	127	21	4.3·10^{-4}
25ºC-75ºC											
Cold (BTC)	1.32	7.14	2.64·10^{-5}	0.88	506.87	514.01	0.024	0.48	139	145	6.3·10^{-4}
Hot (BTC)	0.71	0.59	2.68·10^{-5}	0.95	86.77	87.36	0.074	0.44	143	90	8.5·10^{-4}
Cold (ATC)	1.33	20.13	4.38·10^{-5}	0.78	152.50	172.63	0.002	0.49	152	26	5.9·10^{-4}
Hot (ATC)	0.73	2.18	2.17·10^{-5}	0.97	114.69	116.87	0.035	0.41	155	213	8.9·10^{-4}
25ºC-100ºC											
Cold (BTC)	1.32	7.14	2.64·10^{-5}	0.88	506.87	514.01	0.024	0.48	139	145	6.3·10^{-4}
Hot (BTC)	0.59	0.94	2.94·10^{-5}	0.96	204.94	205.88	0.098	0.48	113	123	7.6·10^{-4}
Cold (ATC)	1.21	7.58	2.47·10^{-5}	0.95	108.60	116.18	0.002	0.45	142	23	7.7·10^{-4}
Hot (ATC)	0.61	1.14	2.59·10^{-5}	0.99	63.01	64.15	0.025	0.45	137	143	1.9·10^{-3}

Table 5

Electrode	R_S/Ω cm²	R_1/Ω cm²	C_1/F cm⁻²	α_1	R_2/Ω cm²	R_P/Ω cm²	C_2/F cm⁻²	α_2	δ/μm	σ/Ω cm² s⁻¹ᐟ²	χ^2
25ºC-25ºC											
Cold and hot (BTC)	1.69	11.62	$3.41 \cdot 10^{-5}$	0.85	319.94	331.56	0.002	0.44	228	93	$6.8 \cdot 10^{-4}$
Cold (ATC)	1.29	3.50	$1.95 \cdot 10^{-5}$	0.68	102.50	106.00	0.002	0.47	266	53	$1.2 \cdot 10^{-3}$
Hot (ATC)	1.20	8.41	$2.07 \cdot 10^{-5}$	0.83	133.00	141.41	0.005	0.41	133	149	$4.9 \cdot 10^{-3}$
25ºC-50ºC											
Cold (BTC)	1.69	11.62	$3.41 \cdot 10^{-5}$	0.85	319.94	331.56	0.002	0.44	228	93	$6.8 \cdot 10^{-4}$
Hot (BTC)	1.17	4.92	$4.20 \cdot 10^{-5}$	0.89	79.29	84.21	0.078	0.41	130	619	$3.9 \cdot 10^{-4}$
Cold (ATC)	1.68	61.07	$4.87 \cdot 10^{-5}$	0.83	94.78	155.85	0.003	0.46	181	309	$3.7 \cdot 10^{-3}$
Hot (ATC)	1.32	8.14	$2.10 \cdot 10^{-5}$	0.91	266.45	274.59	0.041	0.44	391	527	$7.6 \cdot 10^{-4}$
25ºC-75ºC											
Cold (BTC)	1.69	11.62	$3.41 \cdot 10^{-5}$	0.85	319.94	331.56	0.002	0.44	228	93	$6.8 \cdot 10^{-4}$
Hot (BTC)	0.92	0.64	$2.35 \cdot 10^{-5}$	0.98	127.14	127.78	0.225	0.43	126	620	$9.7 \cdot 10^{-4}$
Cold (ATC)	1.61	21.88	$3.64 \cdot 10^{-5}$	0.85	205.00	226.88	0.009	0.45	151	228	$3.2 \cdot 10^{-3}$
Hot (ATC)	0.90	1.28	$2.19 \cdot 10^{-5}$	0.94	152.70	153.98	0.051	0.43	384	308	$1.8 \cdot 10^{-3}$
25ºC-100ºC											
Cold (BTC)	1.69	11.62	$3.41 \cdot 10^{-5}$	0.85	319.94	331.56	0.002	0.44	228	93	$6.8 \cdot 10^{-4}$
Hot (BTC)	0.66	1.49	$3.13 \cdot 10^{-5}$	0.96	58.36	59.85	0.011	0.46	260	507	$6.6 \cdot 10^{-4}$
Cold (ATC)	1.56	21.69	$4.49 \cdot 10^{-5}$	0.88	56.09	77.78	0.001	0.53	139	262	$9.5 \cdot 10^{-3}$
Hot (ATC)	0.69	3.74	$3.30 \cdot 10^{-5}$	0.96	83.75	87.49	0.008	0.47	361	553	$8.6 \cdot 10^{-4}$

Figure 1
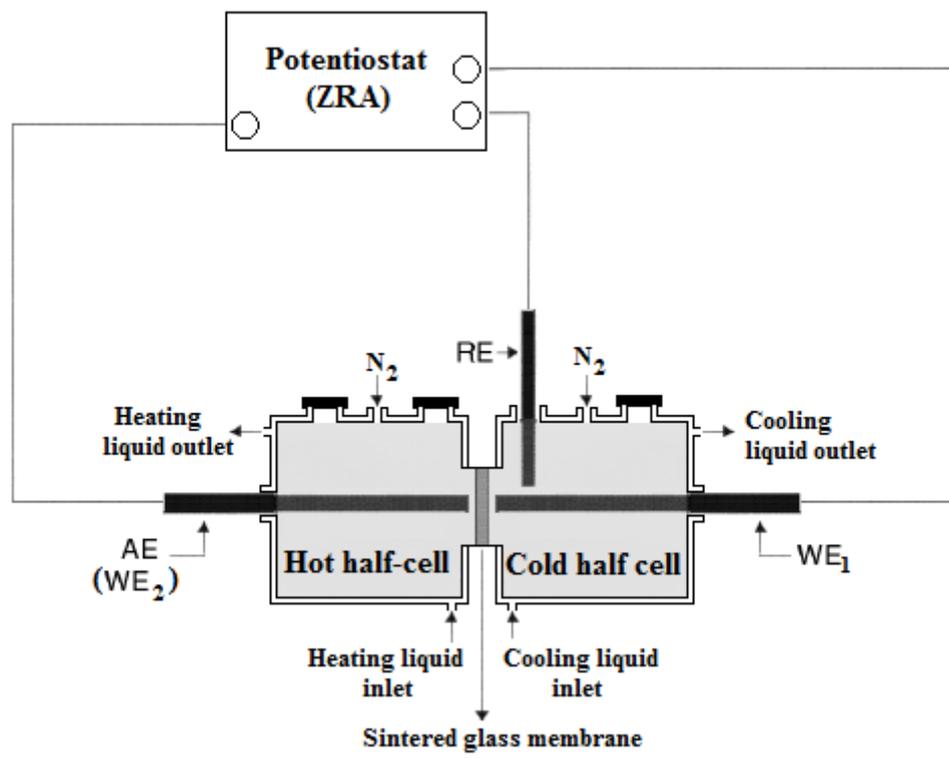
Figure 2
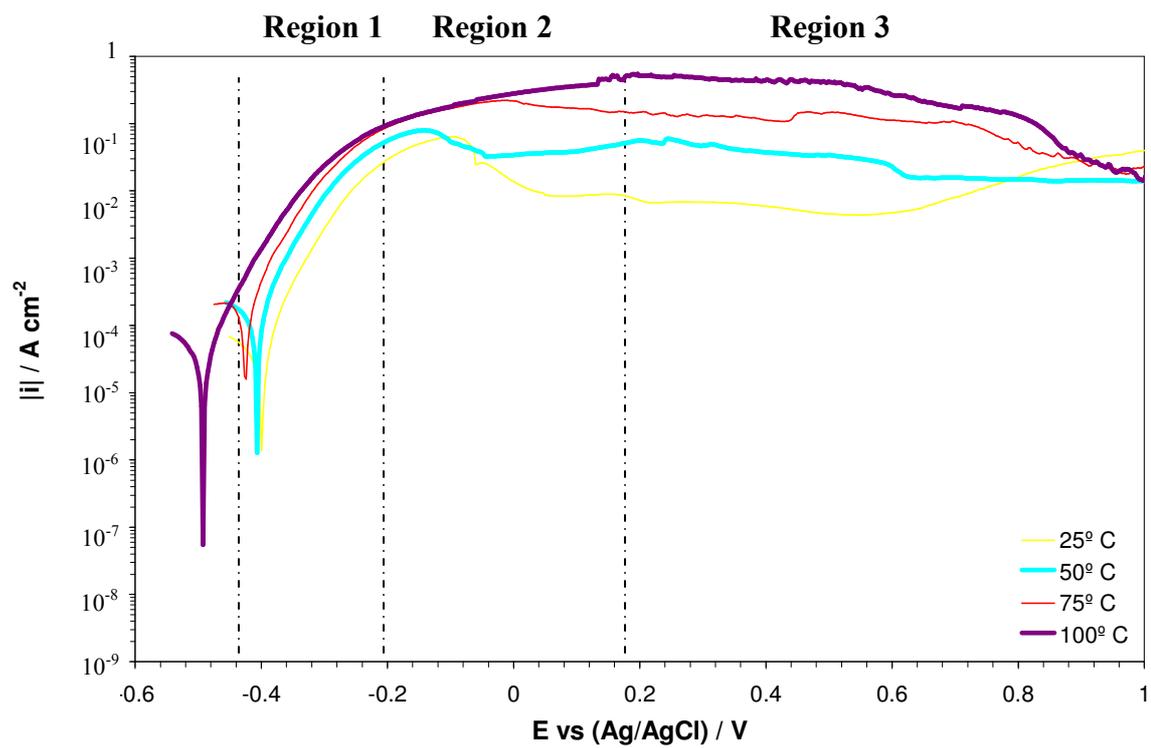
Figure 3
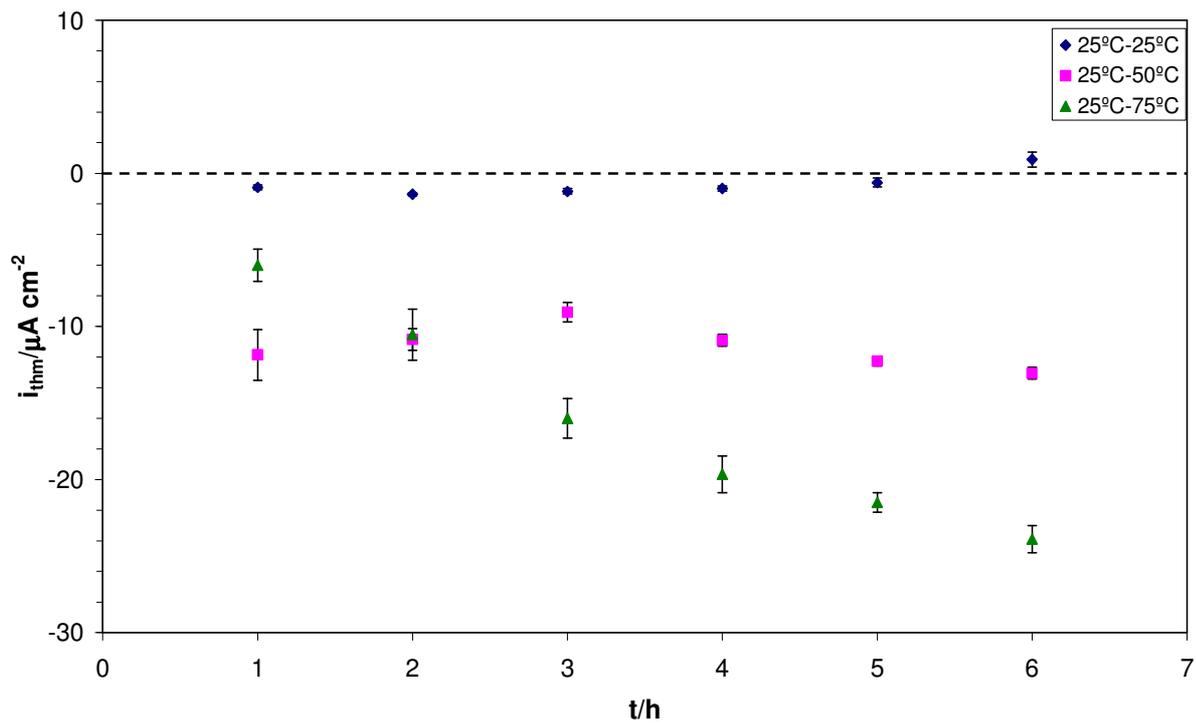
(a)
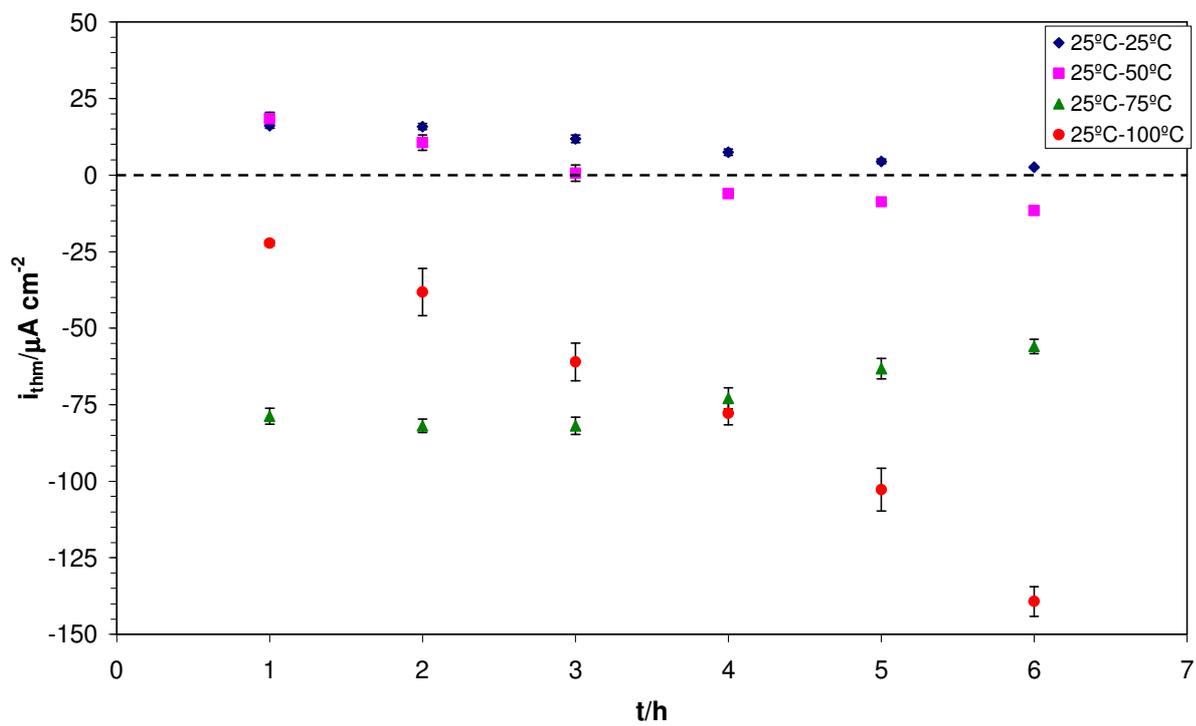
(b)
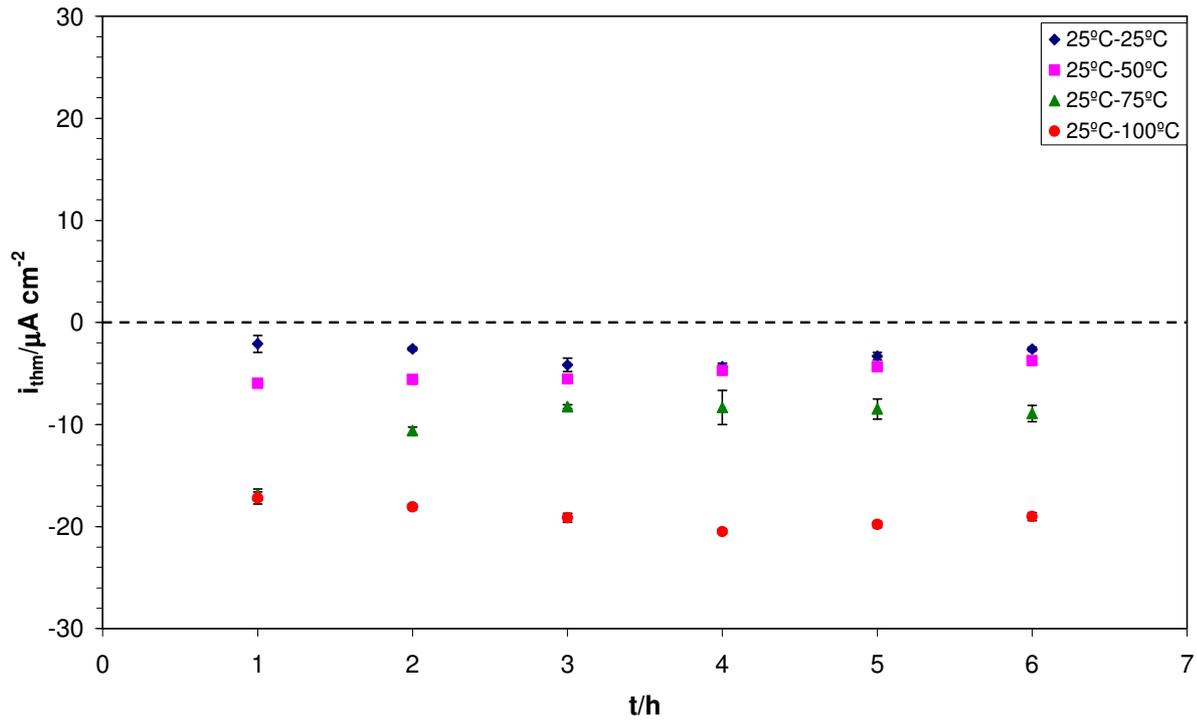
(c)

Figure 4
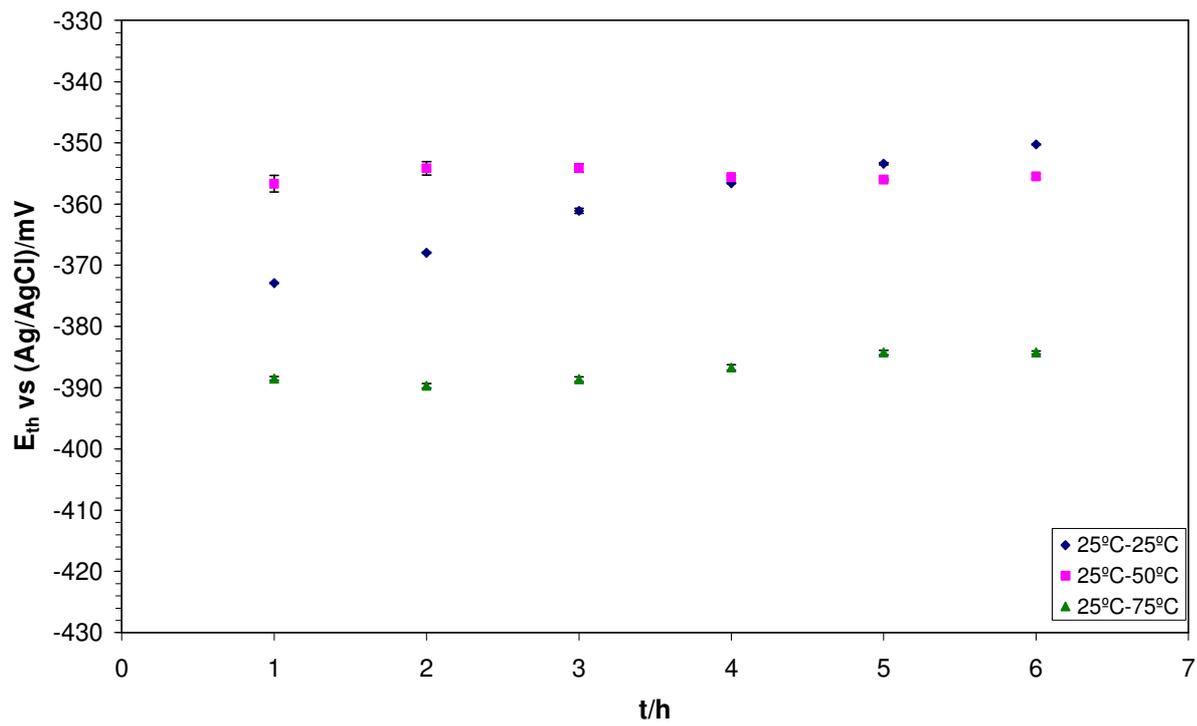
(a)
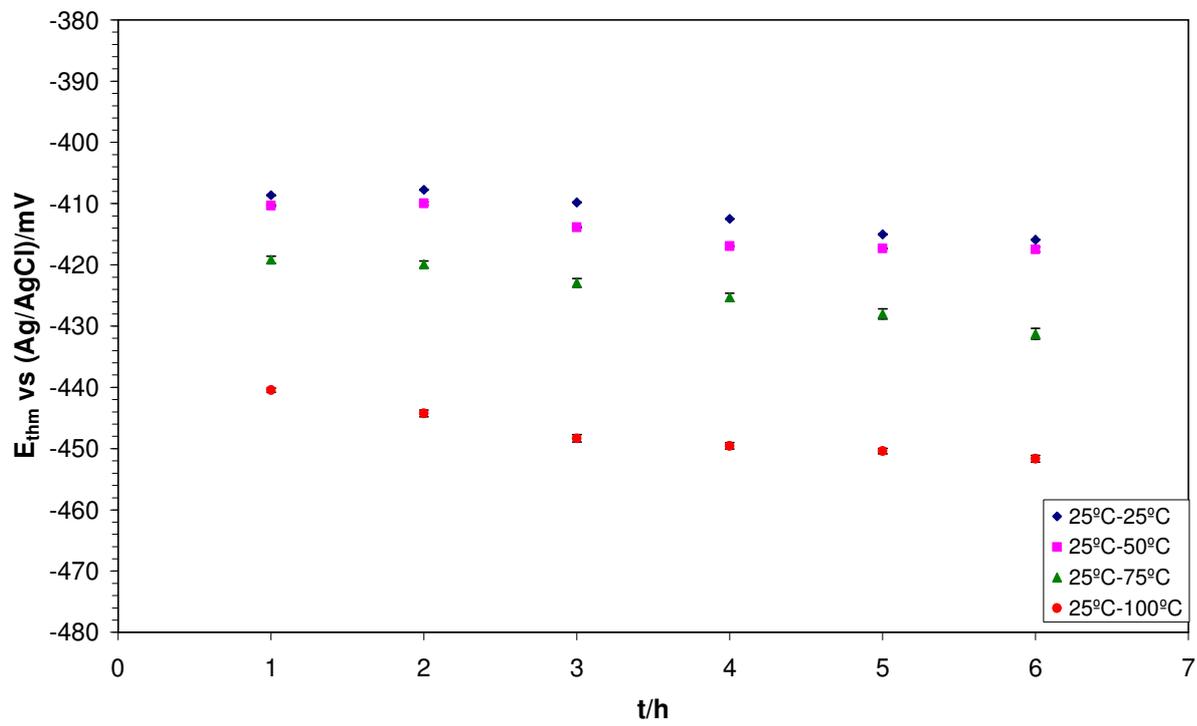
(b)
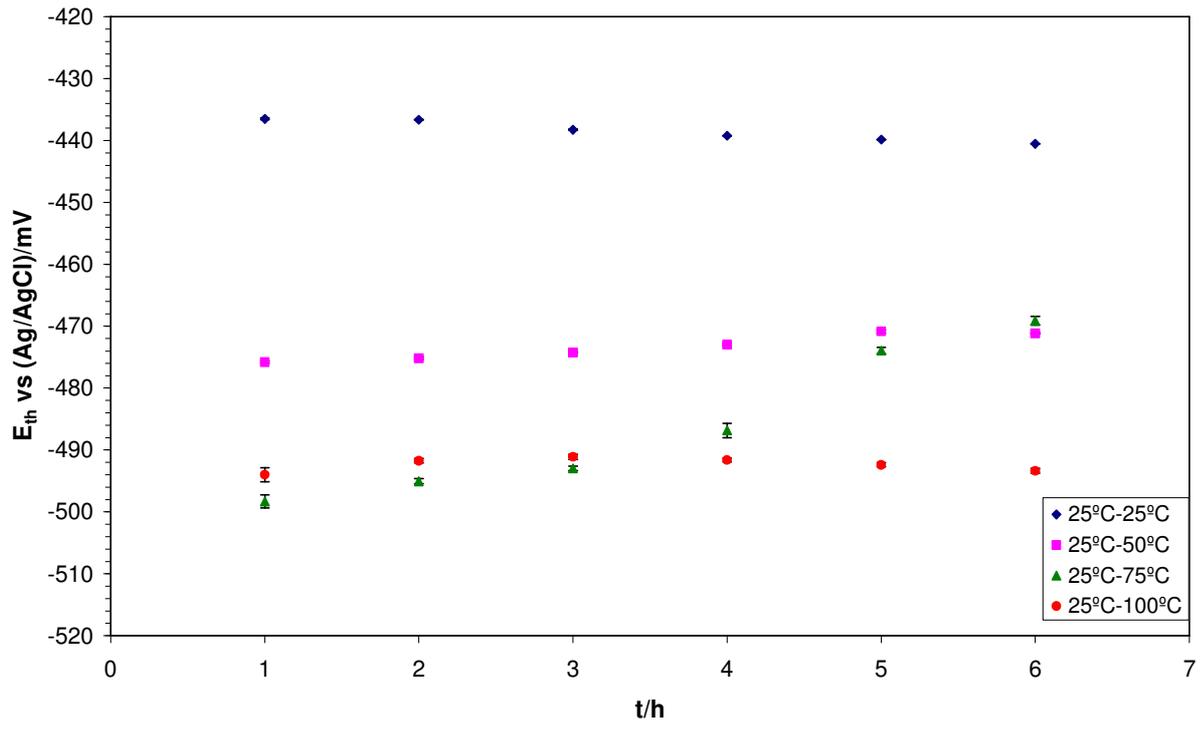
(c)

Figure 5
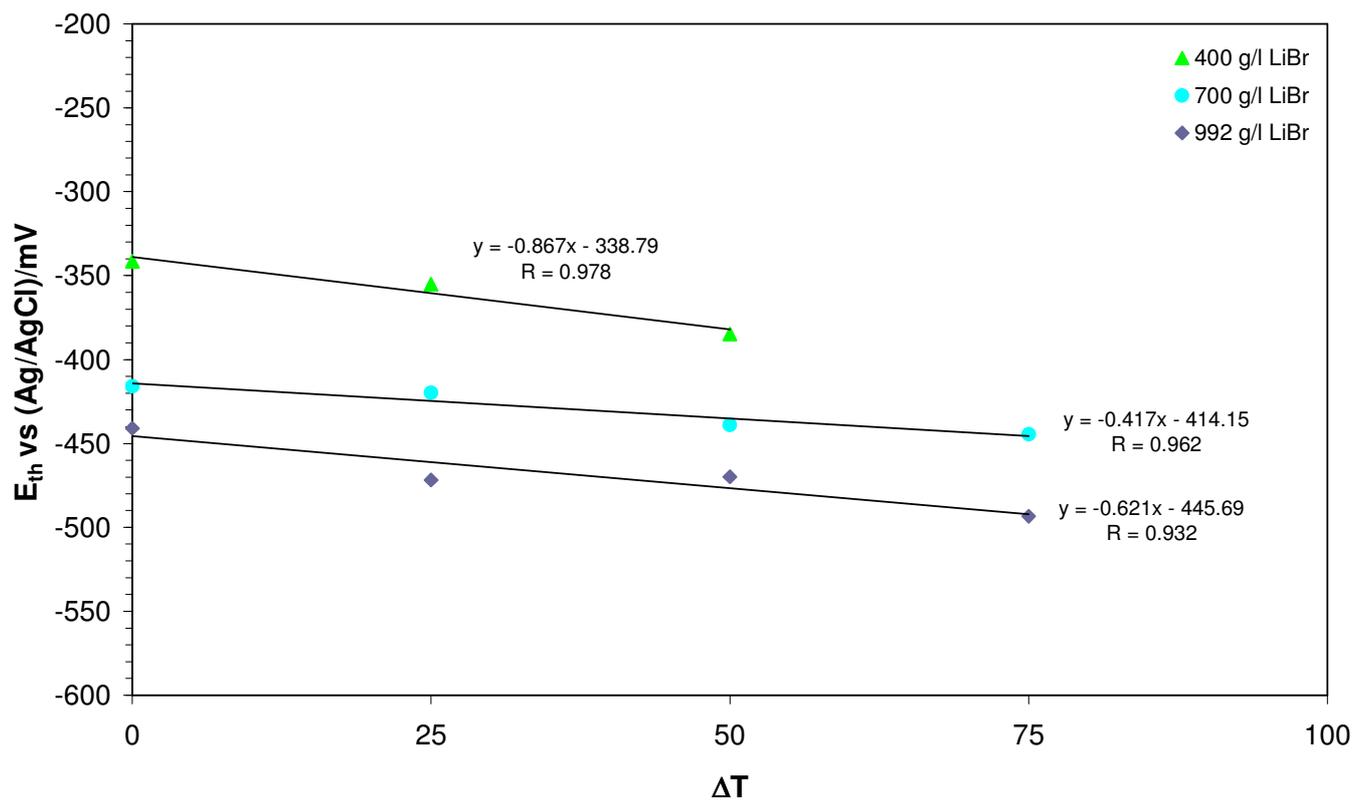
Figure 6

(a)

(b)

(c)

(d)

Figure 7

Figure 8